Electronic transport properties of quantum-well states in ultrathin Pb (111) films

Nobuhiro Miyata,* Kotaro Horikoshi, Toru Hirahara, and Shuji Hasegawa
Department of Physics, School of Science, The University of Tokyo, 7-3-1 Hongo, Bunkyo-ku, Tokyo 113-0033, Japan

C. M. Wei
Institute of Atomic and Molecular Sciences, Academia Sinica, Taipei 106, Taiwan 11529, Republic of China

Iwao Matsuda
Synchrotoron Radiation Laboratory, The Institute for Solid State Physics, The University of Tokyo, 5-1-5 Kashiwanoha, Kashiwa 277-8581, Japan

(Received 20 June 2008; revised manuscript received 16 September 2008; published 4 December 2008)

Electrical conduction mechanism in ultrathin Pb (111) films formed on the Si(111)$\sqrt{3}\times\sqrt{3}$-Pb surface has been investigated by means of *in situ* conductivity measurements, angle-resolved photoemission spectroscopy, and first-principles calculations. To investigate the origin of the bilayer oscillation observed in the present conductivity measurement, we perform some simulations based on the calculated band structure. They reveal that the density of states near the Fermi level cannot explain the bilayer oscillation, therefore, exclusively assigning it to the relaxation time. Surface roughness during the bilayer film growth seems to play a crucial role in the bilayer oscillation of the relaxation time.

DOI: 10.1103/PhysRevB.78.245405 PACS number(s): 73.21.Fg, 73.50.−h, 71.15.Nc

I. INTRODUCTION

Quantum oscillations in ultrathin Pb films have been an intriguing topic among surface or nanoscience communities. When the film thickness d approaches the Fermi wavelength, quantum confinement becomes important in the physical properties.[1] The confinement of conduction electrons by the vacuum on one side and the interface on the other side gives rise to quantum-well (QW) states. For most of s-p metals, the energy dispersion is nearly parabolic. As d increases, the number of QW states increases and the subbands drop below the Fermi level E_F one by one. Because this E_F crossing is periodic, various physical properties oscillate as a function of d: film stability,[2–5] electrical conductivity,[6–9] critical temperature,[10,11] and critical magnetic field[12,13] of superconductivity, etc. In most of these previous studies, the experimental results have been interpreted by the oscillation of the density of states at E_F. However, the band structure has not been fully taken into account in the discussion. Recent angle-resolved photoemission spectroscopy (ARPES) measurements, which have been powerful experimental techniques to measure the band structure, revealed that an ultrathin Pb film exhibits unusual band dispersion which cannot be regarded as parabolic.[14–16] Moreover, the importance of the band structure in the whole k space was also suggested in the theoretical point of view.[17]

Electrical conductions are essentially scattering events of carriers associated with interband or intraband excitations of electrons at E_F, and it is governed by the number of carriers (electrons) and scatterers (phonons, impurities, and boundaries). In the framework of the Drude model, expressed as $\sigma=ne^2\tau/m$, conductivity σ is given by electron density n (the number of carriers) and relaxation time τ (the inverse of scattering time) (e and m are electron charge and mass, respectively). This means that σ depends on both the numbers of electrons and scatterers. Our concern is whether n or τ is the origin of the bilayer periodicity observed in electron transport. Therefore, in the present paper, we have studied the electron-transport property and electronic structure of ultrathin Pb films prepared on the Si(111)$\sqrt{3}\times\sqrt{3}$-Pb surface, both experimentally and theoretically. In simulations from the calculated Fermi surface and band structure, we find that n does not have any bilayer dependences. Therefore, the measured bilayer oscillation is exclusively assigned to change in τ. Furthermore, the factor that determines τ is investigated and surface roughness during the bilayer film growth seems to play a crucial role.

II. EXPERIMENTAL AND CALCULATION METHODS

The measurements were performed in ultrahigh vacuum chambers. The base pressure was 1×10^{-10} Torr. An n-type (P-doped, 1–10 Ω cm) Si(111) wafer was chosen as the substrate. After preparing a clean Si(111)7×7 surface by resistive heating, Pb was deposited on the surface. The evaporation of Pb was done by a graphite effusion cell. About 1 ML of Pb deposition and subsequent annealing at 700 K for a few minutes made the Si(111)$\sqrt{3}\times\sqrt{3}$-Pb surface (1/3 $\mathrm{ML_{Si}}$, 1 $\mathrm{ML_{Si}}=7.83\times10^{14}$ $1/\mathrm{cm^2}$). Further Pb deposition on this surface at 120 K yielded detection of QW states of each atomic layer.[18] In this paper, atomic layer of Pb (111) denotes 1 ML=2.86 Å. Cleanliness and crystallinity of all surfaces were checked by reflection high-energy electron diffraction. The conductivity measurements were performed by two kinds of methods. One is a four-terminal (FT) method which has macroscopic probe spacing. The current flows through the tantalum clamps and voltage is measured by the two inner probes.[19] The probe spacing was ~2 mm. The other is a micro-four-point-probe (MFPP) method. The current flows through two outer probes and voltage is measured by two inner probes.[20] The probe spacing was 20 μm. The schematic views of the FT and MFPP measurements are shown in the insets of Figs. 1 and 2, respectively. The ARPES experi-

 ©2008 The American Physical Society

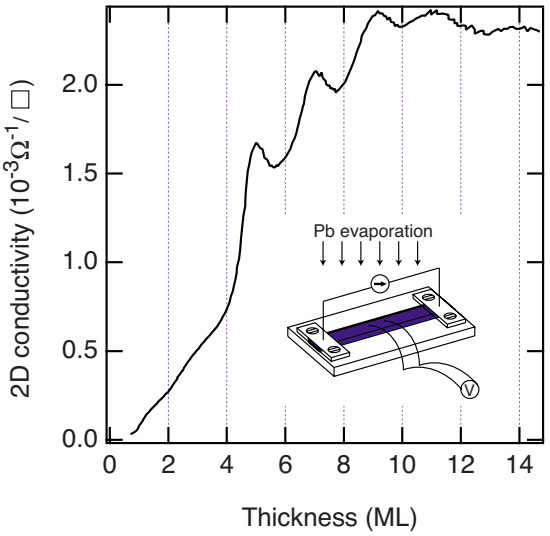

FIG. 1. (Color online) Two-dimensional (2D) conductivity during Pb deposition at 130 K measured by a FT method. The inset shows a schematic view for configuration around the sample. The probe spacing is ~2 mm.

ment was performed at the laboratory. Unpolarized He $I\alpha$ radiation ($h\nu$=21.22 eV) and a commercial electron spectrometer (Scienta SES-100) were used. Band dispersion and Fermi surfaces were obtained by rotating a sample in polar and azimuthal angles. The calculations were carried out using the Vienna *ab initio* simulation package (VASP) (Ref. 21) based on density-functional theory with projector augmented-wave pseudopotentials[22] and plane waves. We have employed the Perdew-Burke-Ernzerhof exchange-correlation approximation.[23] The detail can be found in Refs. 17 and 24. All the calculations shown in this paper were done for free-standing Pb slabs separated by a vacuum region. The calculation of the band structure for bulk Pb has been done in a similar manner.

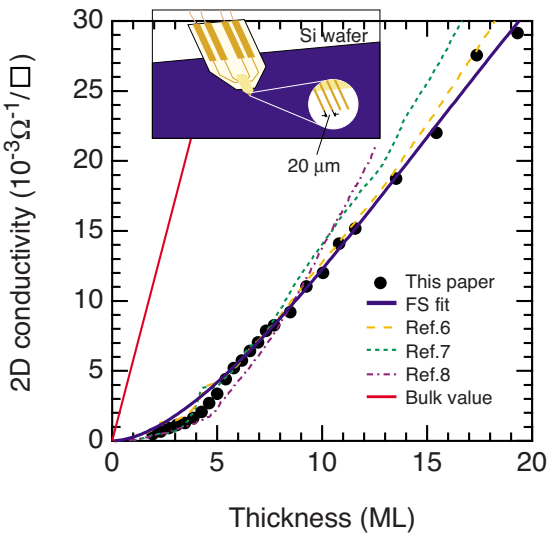

FIG. 2. (Color online) 2D conductivity as a function of thickness measured by a MFPP method. The thin solid curve is the fitting curve with the Fuchs-Sondheimer (FS) formula. The inset represents MFPP approaching the Si substrate. The probe spacing is 20 μm. The results of Refs. 6–8, and bulk Pb value (the straight line) at 80 K are also shown.

III. RESULTS

A. Conductivity measurements

In the present paper, we show 2D conductivity instead of three-dimensional (3D) conductivity. Conversion from the measured resistance to the 2D conductivity is as follows. We consider that the measurement current in principle flows through three channels in the sample: (1) quantum-well states in ultrathin films, (2) bulk states in the space-charge layer, and (3) bulk states in the interior crystal.[25] In the FT and MFPP methods, contribution from channel (2) can be neglected because it is much smaller than that from channel (1). In the FT method, contribution from channel (3) is essentially included in the raw data so we extracted the film conductivity from the measured resistance. First, we measured the resistance before and during deposition. Second, we converted the resistance R to the 2D conductivity σ_{2D} through the relation $\sigma_{2D}=(1/R)(l/w)$, where l and w are the sample length and width, respectively. Finally we obtained the film conductivity by subtracting the conductivity before deposition. In the MFPP method, on the other hand, as they are sensitive enough to measure the film conductivity, channel (3) can be neglected. We converted the measured resistance to the 2D conductivity through the relation $\sigma_{2D}=\ln 2/(\pi R)$.[26]

Figure 1 shows a thickness dependence of σ_{2D} obtained by the FT measurement at 130 K. The measurement was performed continuously during Pb deposition. Up to 4 ML, σ_{2D} is low and increases monotonically. Above 4 ML, σ_{2D} increases rapidly and begins to oscillate and shows peaks at 5, 7, 9, and 11 ML. A similar oscillation in conductivity was also observed in Ref. 7, although the substrate surface structure was different. This trend is consistent with the scanning tunneling microscopy (STM) observations, in which Pb does not fully cover the whole surface at $d<4$ ML.[5] The rapid increase at 4 ML was observed in the previous conductivity experiments.[7,8] Despite the difference of the surface of the substrate [Si(111)$\sqrt{3}\times\sqrt{3}$-Pb in the present experiment and Si(111)6×6-Au,[6] Si(111)$\sqrt{3}\times\sqrt{3}$-Ag,[7] and Si(111)7×7[8] in the previous experiments], a similar thickness dependence was observed.

Figure 2 shows the result of the MFPP measurement at 80 K. In contrast to the FT measurement shown in Fig. 1, an oscillation of σ_{2D} was not observed. For comparison the value of bulk Pb at 80 K and the previous results from Ref. 6 (at 110 K), Ref. 7 (at 20 K), and Ref. 8 (at 15 K) are also shown by a thin solid line and broken lines, respectively. The conversion from the 3D conductivity σ_{3D} to σ_{2D} was performed through the relation $\sigma_{2D}=\sigma_{3D}\times d$. Despite the different temperature and different surface of the substrate, all the data of σ_{2D} follow almost the same thickness dependence. Also, these experimental values are much smaller than the calculated value from the bulk conductivity. This is probably because surface roughness scattering is dominant rather than phonon and interface scattering.

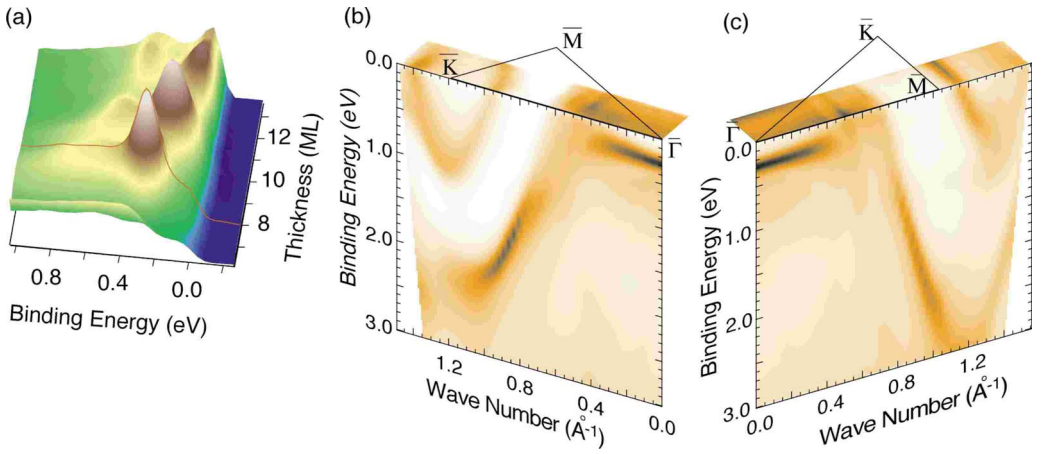

FIG. 3. (Color online) (a) Photoemission intensity at $\bar{\Gamma}$ as a function of thickness and binding energy. Orange highlight shows the spectra for an 8 ML film, the electronic structure of which is shown in detail in (b) and (c). Band structure from (b) $\bar{\mathrm{K}}$ to $\bar{\Gamma}$ and (c) from $\bar{\Gamma}$ to $\bar{\mathrm{M}}$ directions.

We performed fitting of the experimental data by the FS formula.[27] The FS formula, which is a classical description for thin metal films, incorporates diffusive scattering at the surface or interface by a phenomenological specular parameter p. $p=0$ and 1 corresponds to diffusive and specular scatterings at the surface and interface, respectively. In the case $l_B \ll d$ where l_B is the carrier mean-free path in bulk, the FS formula reduces to

$$\sigma_{2D} = \frac{3}{4}\sigma_0 \frac{1+p}{1-p}\frac{d^2}{l_B}\ln\left(\frac{l_B}{d}\right), \tag{1}$$

where σ_0 is the 3D bulk conductivity. In the fitting, the bulk value at 80 K (Ref. 28) was used as σ_0, and p and l_B were used as fitting parameters. The fitting results are $p=0$ and $l_B=190$ Å, which are shown by a thick solid line in Fig. 2. The film thickness (≤ 60 Å) is much shorter than l_B, which is consistent with the picture that scattering by surface roughness is dominant in transport. The deviation from the fitting curve in the thin thickness region ($d<5$ ML) is due to the discontinuous film structure.[5]

Prior to discussion of the origins of the bilayer oscillation, the difference between the FT and MFPP methods should be mentioned. In the FT method, the measurements were performed continuously during Pb deposition, while in the MFPP method, the measurements were performed discontinuously after step-by-step Pb deposition. Therefore, in spite of higher sensitivity of MFPP technique to the properties of the thin films, data points of the FT method were much more than that of the MFPP method, and it enabled one to detect a bilayer oscillation. As the references to support this explanation, a bilayer oscillation was observed in continuous measurements[6,7] while it was not in discontinuous measurement.[8,9]

B. ARPES measurements and band calculation

To discuss the electron-transport phenomena and oscillatory behavior, the band structure in the whole 2D k space is needed. The 3D plot in Fig. 3(a) shows the normal-emission intensity of photoemission as a function of the film thickness and binding energy. Three major peaks at binding energies of 0.26, 0.15, and 0.06 eV below E_F attain their maximum intensities at 8, 10, and 12 ML, respectively. As an example of the band structure, Figs. 3(b) and 3(c) show the valence-band dispersion images for the 8 ML film from $\bar{\mathrm{K}}$ to $\bar{\Gamma}$ and from $\bar{\Gamma}$ to $\bar{\mathrm{M}}$ directions, respectively. The photoemission intensity distribution in k space at E_F is shown in detail in Fig. 4(b). The intensity increases from white (minimum) to black (maximum). Similar to previous reports,[14–16] the band dispersion from $\bar{\Gamma}$ at 0.25 eV below E_F is not parabolic but almost flat. According to Ref. 16, this flat band is reproduced better by including the effect of spin-orbit coupling in the first-principles calculation. Around $\bar{\mathrm{K}}$ and $\bar{\mathrm{M}}$, in contrast, dispersive bands are observed. The calculated band dispersion shown in Fig. 6(a) roughly reproduces the experimental results shown in Figs. 3(b) and 3(c), although the experimental dispersion does not resolve the multiple bands around $\bar{\mathrm{M}}$ and $\bar{\mathrm{K}}$ points. Only one weakly dispersive subband is observed around $\bar{\Gamma}$, while the calculation shows more subbands at high binding energy. We do not understand why the deeper subbands are absent in the experimental results.

Figure 4(a) is the calculated 2D Fermi surface for an 8 ML film in the surface Brillouin zone (SBZ) of the Pb (111) surface. 12 QW states (named Q1–Q12) form 14 enclosed

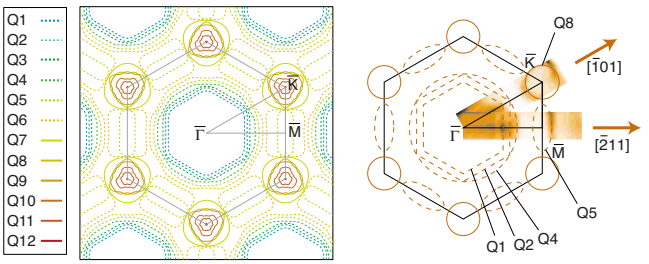

FIG. 4. (Color online) (a) The calculated and (b) experimental 2D Fermi surfaces for an 8 ML film in the surface Brillouin zone of the Pb (111) surface. Dashed and solid lines represent hole and electron pockets, respectively.

TABLE I. The experimental values of the Fermi wave number k_F and Fermi velocity v_F in the $\overline{\Gamma K}$ direction and partial conductivity σ_{2D,Q_s} for the QW states of an 8 ML ultrathin Pb film. k_F is the distance from the symmetry points which is the center of the 2D Fermi surfaces.

				Q7		
Band	Q1	Q2	Q4	$\overline{M\Gamma}$	$\overline{MK}$	Q8
k_F (Å^{-1})	0.48	0.58	0.64	0.08	0.25	0.25
v_F (10^6 m/s)	0.91	0.86	1.1	0.37	0.13	0.77
σ_{2D,Q_s} (10^{-4} $\Omega^{-1}/\square$)	5.1	5.8	8.3	1.2		3.2

Fermi surfaces, where Q5 and Q6 form twofold Fermi surfaces around $\bar{\Gamma}$ and $\bar{M}$. Consequently, the 2D Fermi surfaces consist of six hole pockets around $\bar{\Gamma}$ (Q1–Q6), two hole pockets around $\bar{M}$ (Q5, Q6), and six electron pockets around $\bar{K}$ (Q7–Q12). Figure 4(b) shows the photoemission intensity distribution at E_F. There are three hole pockets around $\bar{\Gamma}$, one hole pocket around $\bar{M}$, and one-electron pocket around $\bar{K}$. Compared with the k value of the calculation, we assign the experimentally observed QW states to Q1, Q2, Q4, Q5, and Q8 [see Fig. 4(b)]. Because k_F of Q3 (0.61 Å^{-1}) is very close to that of Q2 (0.59 Å^{-1}), Q3 was not distinguished from Q2. The distances of k_F from Q4 to Q5 and from Q9 to Q12 are also narrow, thus, Q5 and Q9–Q12 might not be distinguished either. Q5, forming two Fermi surfaces, are observed only in the second SBZ and not in the first SBZ. This might be due to the so-called photoemission structure factor.[29,30] It is an open question why Q6, which also forms two Fermi surfaces, are not observed in both the first and second SBZs.

We perform a simple estimation of σ_{2D} for an 8 ML film from the ARPES measurement. The relation between σ_{2D} and band structure is given by the Boltzmann equation as an integral containing the velocity tensor of $v_{ki}v_{kj}$, where $v_{ki}=(1/\hbar)(\partial E/\partial k_i)$ is the velocity along i direction. Assuming a constant relaxation time $\tau(\boldsymbol{k})=\tau$ that is irrespective of electron wave vector $\boldsymbol{k}$, the conductivity in i direction is represented by

$$\sigma_{2D} = \frac{1}{2\pi^2}\frac{e^2\tau}{\hbar}\oint \frac{v_{ki}^2}{|v_k|}dk_F. \tag{2}$$

The value of τ is taken from the Hall measurement in Ref. 9 ($\tau \sim 3\times 10^{-15}$ s). k_F and v_F is estimated by a linear fit to the calculated and experimental band dispersions. The shapes of the 2D Fermi surfaces of the respective subbands Q_s are simply assumed to be a hexagon, circles, and an ellipse [see the schematic views illustrated in Fig. 4(b)]. Subsequently, σ_{2D} from each band was obtained from Eq. (2). The values of k_F, v_F, and partial conductivity σ_{2D,Q_s} are summarized in Table I. The total conductivity is $\sigma_{2D}=2.3\times 10^{-3}$ $(\Omega^{-1}/\square)$. We compared this σ_{2D} with the conductivity in the MFPP experiment because MFPPs can quantitatively measure the value of film conductivity, which is in contrast to the FT method that includes possible contributions from the substrate. Whereas the estimation is simplified, this value is comparable to the one in the MFPP conductivity measurement, $\sim 8\times 10^{-3}$ $(\Omega^{-1}/\square)$ (see Fig. 2). This difference of the values can be attributed to that of the number of the observed QW bands between the ARPES experiment and band calculation. It is noted that contributions from the enclosed Fermi surfaces around the symmetry points ($\bar{\Gamma}$, $\bar{K}$, and $\bar{M}$) are comparable to each other. Moreover, the mean-free path $l_F=v_F\tau \sim 10$–30 Å, where τ is the value taken from Ref. 9. This value is roughly equal to the film thickness (8 ML $\sim$ 20 Å), which is consistent with the picture that surface roughness governs the film property.

IV. DISCUSSION

It is understood that the importance of surface roughness has been suggested in the experiments. As the origin of the oscillation, (a) n of mobile electrons, (b) τ determined by intersubband transition, and (c) τ determined by surface roughness with bilayer growth are considered in the framework of the Drude model. (a) was used to explain some of the previous experiments.[10] The periodic E_F crossing of QW states results in an oscillation of the density of states per area at E_F, $\mathcal{D}^{2D}$. In the case of conductivity, $\mathcal{D}^{2D}$ is related to σ_{2D} through the Boltzmann equation such as $\sigma_{2D}\propto\mathcal{D}^{2D}$.[31] (b) was proposed by Trivedi and Ashcroft,[32] and was discussed in a previous paper.[6] According to them, an oscillation is caused by intersubband scattering between QW states. Considering a thickness dependence of conductivity, the scattering rate $S=1/\tau_{ks}$ (k denotes the wave number and s denotes the index of QW states) increases at certain thicknesses when the number of QW states crossing E_F increases because the number of the scattered states $|k's'\rangle$ increases, such as

$$S = \frac{1}{\tau_{ks}} = \sum_{k',s'} \overline{\langle k's'|W|ks\rangle}, \tag{3}$$

where W denotes the transition rate and overbar denotes an average over disorder. Consequently, the conductivity results in a saw-tooth-like oscillation in the thickness dependence. It is noted that this saw-tooth-like oscillation occurs even if surface roughness does not show bilayer film growth. (c) is a simple picture in which electrons are scattered less diffusively by film surface when the surface is smooth, while they are scattered more diffusively when the surface is not. In contrast to (b), because the film becomes smooth with the bilayer periodicity, τ oscillates as a function of thickness.

First, we investigate the possibility of (a) and find that it is negligible, as described below. $\mathcal{D}^{2D}$ is given as

$$\mathcal{D}^{2D} = \frac{1}{2\pi^2}\oint \frac{dk_F}{|\partial E/\partial k|} \tag{4}$$

$$= \frac{1}{2\pi^2\hbar}\oint \frac{dk_F}{|v_k|}, \tag{5}$$

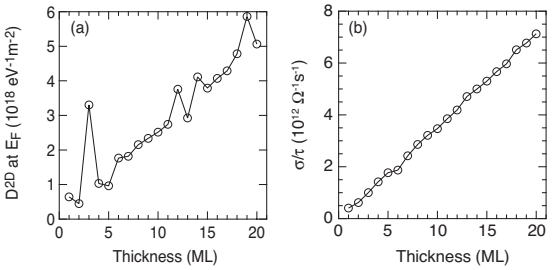

FIG. 5. (a) The calculated $\mathcal{D}^{2D}$ as a function of thickness. $\mathcal{D}^{2D}$ monotonically increases with the exception at 3, 12, 14, and 19 ML. These spikes are originated from QW states at $\bar{\Gamma}$, which form two or more electron/hole pockets at those thicknesses, in contrast to only one hole pocket at other thicknesses. (b) The calculated σ_{2D}/τ as a function of thickness. σ_{2D}/τ also monotonically increases, and no significant oscillation is identified.

where $v_k=(1/\hbar)(\partial E/\partial k)$ is the velocity. Since the shape of the 2D Fermi surface and slope of the band dispersion $\partial E/\partial k$ have been obtained from the first-principles calculation, we can perform a calculation for $\mathcal{D}^{2D}$. Figure 5(a) shows the calculated $\mathcal{D}^{2D}$ as a function of thickness. Although there are spikes at 3, 12, 14, and 19 ML, $\mathcal{D}^{2D}$ increases monotonically and no bilayer oscillation is observed. These spikes are originated from QW states at $\bar{\Gamma}$, which form two or more electron/hole pockets at those thicknesses, in contrast to only one hole pocket at other thicknesses. Furthermore, we perform another calculation for σ_{2D}/τ by using Eq. (2). Figure 5(b) shows σ_{2D}/τ as a function of thickness. The spikes observed in $\mathcal{D}^{2D}$ have smoothed out and σ_{2D}/τ also increases monotonically with thickness. Therefore, we conclude that $\mathcal{D}^{2D}$ cannot be the origin of the bilayer oscillation.

Next, to investigate the possibility of (b), we perform a calculation of the band structure with different thicknesses. This possibility is also denied by investigating a thickness dependence of the number of electron or hole pockets. As an example of this, we present the thickness dependence of the number of hole pockets around $\bar{\Gamma}$. Figure 6(a) shows the band structure for an 8 ML film in the $\bar{\mathrm{K}}$-$\bar{\Gamma}$-$\bar{\mathrm{M}}$ direction. Also plotted in Fig. 6(b) for comparison is the energy dispersion of the bulk Pb in the (111) direction, corresponding to the Γ-L direction. This dispersion determines the energy range for the QW states at $\bar{\Gamma}$. Focusing on the QW states around $\bar{\Gamma}$, Figs. 6(c)–6(f) show the enlarged band structure for 5–8 ML thick films, the area of which is indicated as a dashed square in Fig. 6(a). As one can see, the number of QW states crossing E_F, N, increases from 4 to 5 and from 5 to 6 when d increases from 6 to 7 ML and from 7 to 8 ML, respectively. This result means that N increases one by one with d. N increases in a similar way in the other thicknesses, and we summarize the relation between d and N in the range of 5–15 ML in Fig. 6(g). We have obtained similar results in all the electron or hole pockets around the other symmetry points, $\bar{\mathrm{K}}$ and $\bar{\mathrm{M}}$. Around $\bar{\mathrm{K}}$, N increases one by one with thickness (not shown). Around $\bar{\mathrm{M}}$, N increases by one when d increases from 7 to 8 ML and from 13 to 14 ML (not shown). As a result, the number of QW states crossing E_F in the whole SBZ does not change with the bilayer periodicity;

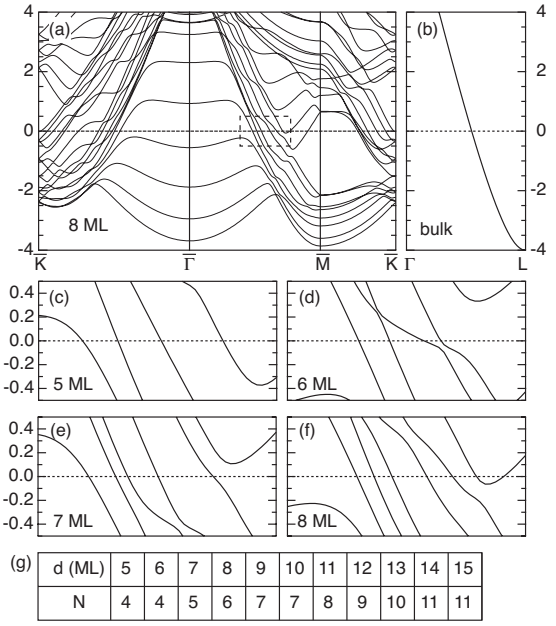

(g)

d (ML)	5	6	7	8	9	10	11	12	13	14	15
N	4	4	5	6	7	7	8	9	10	11	11

FIG. 6. (a) The band calculation for an 8 ML film along the high symmetry lines. (b) The band calculation for bulk Pb in the (111) direction. The enlarged band structure for (c) 5, (d) 6, (e) 7, and (f) 8 ML films [the area is shown in Fig. 6(a) in dashed square]. (g) d and N (number of the hole pockets around $\bar{\Gamma}$ crossing E_F) for 5–15 ML films.

thus, τ determined through intersubband scattering also cannot be the origin of the bilayer oscillation.

From the discussion above, only the possibility of (c) has survived. This indicates that film growth onto Si(111) substrate has some bilayer properties. Unfortunately, such bilayer film growth cannot be confirmed from our experiments and calculations. Comprehensive study of growth morphology by microscopy experiments is desirable. However, it has been known that Pb growth is complicated and there have been some reports of layer-by-layer growth with quasibilayer lattice distortion[4] or bilayer growth.[5] Our conclusion might be related to these bilayer properties in film growth.

V. CONCLUSION

In summary, a bilayer oscillation of electrical conductivity is observed, and analysis of the conductivity and ARPES experiments indicate importance of surface roughness in the oscillation. To investigate it, some simulations are performed from the calculated band structure. $\mathcal{D}^{2D}$ cannot explain this oscillation and τ is exclusively attributed. Moreover, the factor that determines the change in τ cannot be intersubband scattering between QW states; therefore, surface roughness during the bilayer film growth seems to play a crucial role. This might be related to bilayer preference of Pb growth reported in previous experiments.

We would like to emphasize that a description of a bilayer oscillation of σ_{2D} requires full consideration of the band structure. Therefore, it is surprising that superconductivity occurs in ultrathin metal films, which consists of much less electrons than bulk, although superconductivity is a phenom-

enon in which so many electrons with different $\boldsymbol{k}$ should participate. In Ref. 10 the oscillation of critical temperature of superconductivity is explained by $\mathcal{D}^{2D}$ at $\bar{\Gamma}$. This explanation should be valid only when most of electrons that participate in superconductivity originate from the hole pockets around $\bar{\Gamma}$. More comprehensive study for the band structure in the whole k space is desirable for complete understanding.

ACKNOWLEDGMENTS

We are grateful to M. C. Tringides for helpful discussion. We would like to thank Rei Hobara for his assistance with the ARPES experiment. This work has been supported by Grants-In-Aid from Japan Society for the Promotion of Science.

*nmiyata@surface.phys.s.u-tokyo.ac.jp

[1] T.-C. Chiang, Surf. Sci. Rep. **39**, 181 (2000).
[2] M. M. Özer, Y. Jia, B. Wu, Z. Zhang, and H. H. Weitering, Phys. Rev. B **72**, 113409 (2005).
[3] H. Hong, C. M. Wei, M. Y. Chou, Z. Wu, L. Basile, H. Chen, M. Holt, and T.-C. Chiang, Phys. Rev. Lett. **90**, 076104 (2003).
[4] P. Czoschke, H. Hong, L. Basile, and T.-C. Chiang, Phys. Rev. Lett. **91**, 226801 (2003).
[5] M. Hupalo and M. C. Tringides, Phys. Rev. B **65**, 115406 (2002).
[6] M. Jałochowski and E. Bauer, Phys. Rev. B **38**, 5272 (1988); M. Jałochowski, E. Bauer, H. Knoppe, and G. Lilienkamp, Phys. Rev. B **45**, 13607 (1992).
[7] M. Jałochowski, M. Hoffmann, and E. Bauer, Phys. Rev. Lett. **76**, 4227 (1996).
[8] O. Pfennigstorf, A. Petkova, H. L. Guenter, and M. Henzler, Phys. Rev. B **65**, 045412 (2002).
[9] I. Vilfan, M. Henzler, O. Pfennigstorf, and H. Pfnür, Phys. Rev. B **66**, 241306(R) (2002).
[10] Y. Guo, Y. F. Zhang, X. Y. Bao, T. Z. Han, Z. Tang, L. X. Zhang, W. G. Zhu, E. G. Wang, Q. Niu, Z. Q. Qiu, J. F. Jia, Z. X. Zhao, and Q. K. Xue, Science **306**, 1915 (2004).
[11] D. Eom, S. Qin, M.-Y. Chou, and C. K. Shih, Phys. Rev. Lett. **96**, 027005 (2006).
[12] M. M. Özer, J. R. Thompson, and H. H. Weitering, Nat. Phys. **2**, 173 (2006).
[13] M. M. Özer, Y. Jia, Z. Zhang, J. R. Thompson, and H. H. Weitering, Science **316**, 1594 (2007).
[14] M. H. Upton, T. Miller, and T.-C. Chiang, Phys. Rev. B **71**, 033403 (2005).
[15] J. H. Dil, J. W. Kim, Th. Kampen, K. Horn, and A. R. H. F. Ettema, Phys. Rev. B **73**, 161308(R) (2006).
[16] J. H. Dil, T. U. Kampen, B. Hülsen, T. Seyller, and K. Horn, Phys. Rev. B **75**, 161401(R) (2007).
[17] C. M. Wei and M. Y. Chou, Phys. Rev. B **75**, 195417 (2007).
[18] M. H. Upton, C. M. Wei, M. Y. Chou, T. Miller, and T.-C. Chiang, Phys. Rev. Lett. **93**, 026802 (2004).
[19] S. Hasegawa and S. Ino, Phys. Rev. Lett. **68**, 1192 (1992).
[20] T. Tanikawa, I. Matsuda, R. Hobara, and S. Hasegawa, e-J. Surf. Sci. Nanotechnol. **1**, 50 (2003).
[21] G. Kresse and J. Furthmüller, Phys. Rev. B **54**, 11169 (1996).
[22] P. E. Blochl, Phys. Rev. B **50**, 17953 (1994); G. Kresse and D. Joubert, *ibid.* **59**, 1758 (1999).
[23] J. P. Perdew, K. Burke, and M. Ernzerhof, Phys. Rev. Lett. **77**, 3865 (1996).
[24] C. M. Wei and M. Y. Chou, Phys. Rev. B **66**, 233408 (2002).
[25] S. Hasegawa, I. Shiraki, F. Tanabe, R. Hobara, K. Kanagawa, T. Tanikawa, I. Matsuda, C. L. Petersen, T. M. Hansen, P. Boggild, and F. Grey, Surf. Rev. Lett. **10**, 963 (2003).
[26] L. B. Valdes, Proc. IRE **42**, 420 (1954).
[27] K. Fuchs, Proc. Camb. Philos. Soc. **34**, 100 (1938); E. H. Sondheimer, Adv. Phys. **1**, 1 (1952).
[28] G. T. Meaden, *Electrical Resistance of Metals* (Plenum, New York, 1965), p. 16.
[29] E. L. Shirley, L. J. Terminello, A. Santoni, and F. J. Himpsel, Phys. Rev. B **51**, 13614 (1995).
[30] T. Hirahara, I. Matsuda, and S. Hasegawa, e-J. Surf. Sci. Nanotechnol. **2**, 141 (2004).
[31] I. Matsuda, T. Hirahara, M. Konishi, C. Liu, H. Morikawa, M. D'angelo, S. Hasegawa, T. Okuda, and T. Kinoshita, Phys. Rev. B **71**, 235315 (2005).
[32] N. Trivedi and N. W. Ashcroft, Phys. Rev. B **38**, 12298 (1988).